Effect of the initial particle volume fraction on the structure of a drying colloidal deposit

Janine Emile, Hervé Tabuteau

Effect of the initial particle volume fraction on the structure of a drying colloidal deposit

Janine Emile, Hervé Tabuteau*

Institut de Physique de Rennes, CNRS UMR 6521, Université de Rennes 1, Campus de Beaulieu, 35042 Rennes, France

Graphical abstract

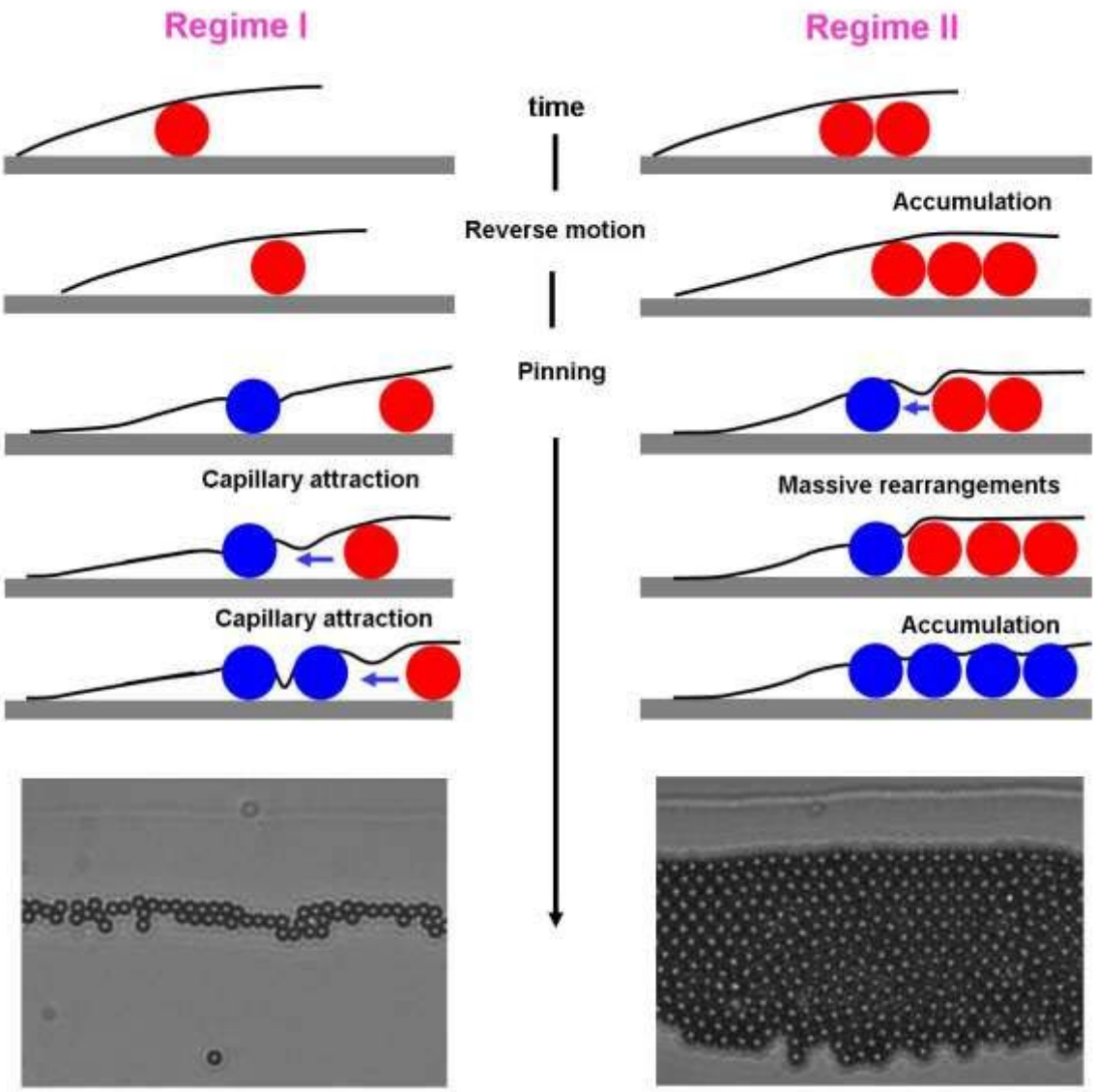

Highlights

- For low volume fractions, below 10^{-4} (regime I), the capillary forces break the colloidal structure.
- For higher particle volume fractions, above 10^{-4} (regime II), the colloidal ring is rigid, pins the contact line and consequently keeps a hexagonal order.

Abstract

During the drying of a droplet on a substrate, dispersed colloidal particles are advected towards the contact line and then accumulate in its vicinity, forming in this way a ring-shaped deposit. Up to now, the structural properties at the particle scale of such pattern have been provided only by its final inspection at the end of the drying process. Here we follow all the stage of the ring formation, up to the complete drying, and for different particle volume fractions. We show that for low particle volume fractions, the final structure of the ring is always disordered, which results only from capillary attraction due to the deformation of the air-water interface. In contrast, for higher particle volume fractions, above 10^{-4}, different consecutive rearrangements lead eventually to the formation of a ring with an ordered structure.

Keywords:
Meniscus deformation; colloidal assembly; capillary attraction; order to disorder transition

*Corresponding author.
E-mail address: herve.tabuteau@univ-rennes1.fr

1. Introduction

The drying of a colloidal suspension droplet on a substrate leads to the formation of various patterns [1] including the so called *coffee-ring* [2,3], extensively studied in a wide range of phenomena (see the review of Sefiane [4]). For particle volume fractions $\phi \geq 10^{-2}$, the scenario of the coffee ring formation is the following. We first observe the spreading of the droplet on a solid surface, motion which stops when some particles draw near the contact line (CL), driven by the evaporative flux, and pin it [5]. There is a depletion distance between the CL and these particles, ruled by the contact angle and the particle size [6]. Thereafter, some particles start to accumulate near the CL slowly enough to form here a crystal. Even later on, the particle velocity near the CL increases rapidly and the rate of particle deposition is so high that the particles can pile up only in a disordered manner [7]. At the end of the drying process, we get a thick and multiple layers ring with a high particle concentration. The liquid drainage within this ring is supposed to not modify its final structure [7]. However, this scenario has not been confirmed since the overall dynamics of the ring formation has not been monitored so far. Studies have focused either on the early times [5,6,8] or on the latest stage of the drying process, when all the solvent is evaporated [6,7].

In the very dilute regime, for ϕ between 10^{-6} and 10^{-2}, the morphology of the final deposit is quite different. Initially, the suspension droplet spreads on the solid surface until it reaches a maximum contact diameter and gets pinned. Then there are successive depinning and pinning events, which lead to the formation of multiple rings [9–12]. Kaplan and Mahadevan developed a theory that couples the liquid flow inside the deposit and the evolution of the shape of the air-water interface near the deposit [11]. They showed that all the different features of deposit can be explained by using only two parameters, ϕ and the inverse capillary number. Their theory also describes the transition from multiple rings, at low ϕ, to a single ring for higher ϕ. However there is no experimental works that confirm their theory, especially the dynamics of such transition. In addition, the possible influence of the structural properties of the ring on such processes has also not been investigated. Finally no one has studied these phenomena at the particle scale so far, in order to make the link between the macroscopic flow and the particle ordering within the deposit.

Here, we study the influence of ϕ, over an extended range (10^{-6} to 5.10^{-3}), on the overall formation of the colloidal ring. Our aim is to determine the dynamics of the ring formation at the particle scale in order to define the influence of both the colloidal assembly and the air-

water interface on such process. We also discussed the relevance of the so called *rush hour effect* on the structural transition observed inside the deposit.

2. Experimental methods

A droplet formed with a micro-syringe (volume 0.60±0.05µL) is deposited on a glass microscope slide and viewed through a SCMOS camera (Hamamatsu Orca Flash 4.0) connected to an inverted microscope (LEICA DMI 3000). Such a low injected volume allows us to study the formation of a single ring during the droplet drying. We get sessile droplets with a diameter roughly equals to 1mm at the base of the cap at the beginning of the experiments. Colloidal suspensions are made of sulfate latex spherical particles (diameter D=1.6 and 2µm, Life technologies, USA). They are diluted in pure water, with ϕ in between 3.10^{-6} and 5.10^{-3}. Before each measurement the solution is sonicate for 30 minutes to break eventual aggregates. The evaporation process is performed under ambient air with controlled temperature (20.0±0.5°C) and high relative humidity RH (50±3%). The particle deposition in the vicinity of the CL is followed every 0.5-1s and the images were analysed using ImageJ software. Glass slides are cleaned with Hellmanex (Sigma-Aldrich, diluted 10 times in pure water), acetone, ethanol, rinsed with pure water and dried with clean compressed air. The solvent we used, deionised water for HPLC (Chormanorm, VWR), wets the clean glass slide completely. The microparticles are partially wetted by the solvent since they are hydrophobic (polystyrene latex).

3. Results

In this work, we used suspension droplets with a fixed volume and various volume fractions ϕ. The suspension droplet initially spreads on the solid surface at t=0s and reaches eventually the same maximum contact diameter for the different ϕ used and gets pinned here at t=30s, before colloids arrive and start to pile up near the CL. We distinguish two regimes based on the width of ring obtained at the end of the drying process. For very dilute suspensions ($10^{-6} < \phi < 10^{-4}$, regime I), the final ring is a monolayer composed of 2-4 rows of particles, while for more concentrated solutions, $10^{-4} < \phi < 5.10^{-3}$ (regime II), it can be close to 32-34 rows. We get a monolayer of particles for both regimes except for ϕ=5.10^{-3}. In the following, we mainly focus on the dynamics of the ring formation with a fixed evaporation rate while the influence of the evaporation rate on the ring formation, for a given ϕ, is considered at the end.

3.1 Regime I

We present the overall dynamics of the ring formation for ϕ=6.10^{-5}. At the beginning of the drying process, particles move towards the CL due to the evaporative flux and the first deposited particles lie in average at a depletion distance L_1 from the CL (Fig.1a) as observed previously [5,6,13].

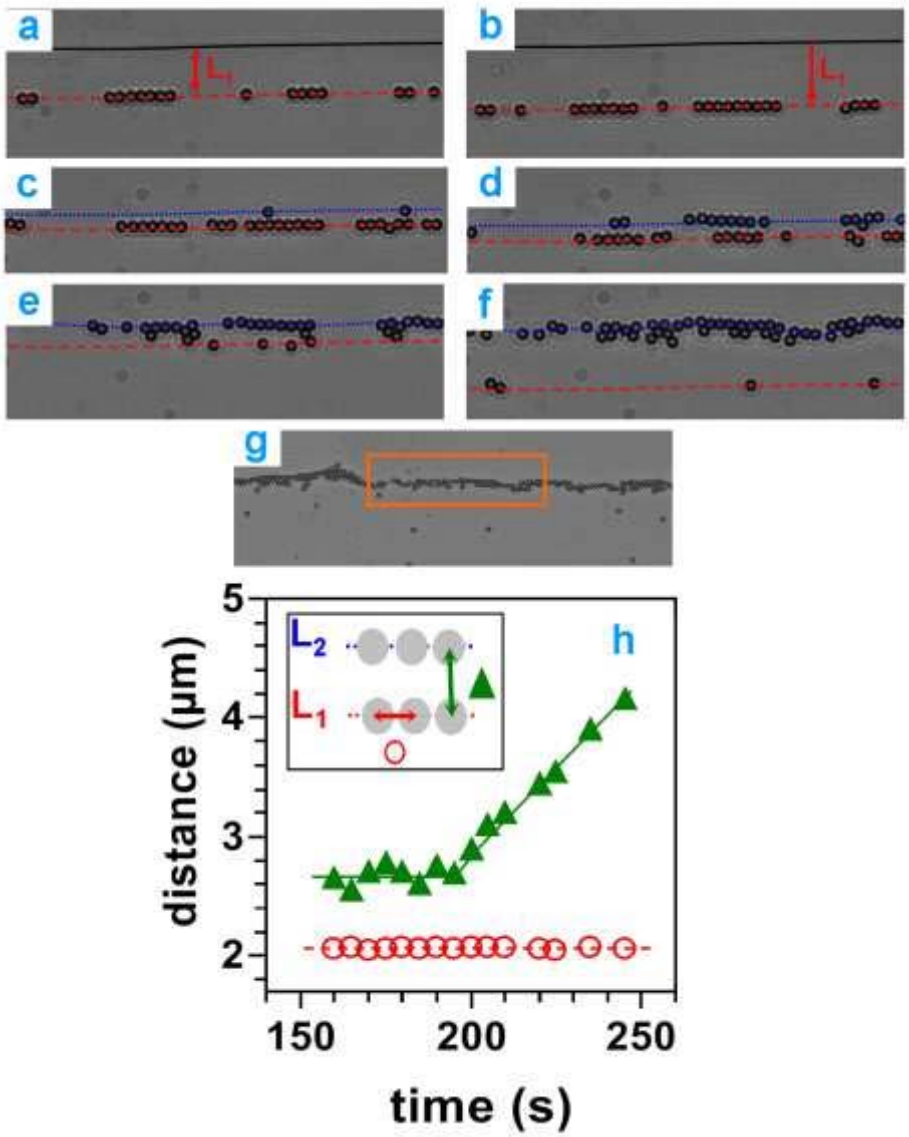

Figure 1: Successive images of the colloidal deposition near the CL for ϕ=6.10^{-5}. The letter for each image (a to f) corresponds respectively to t=105, 150, 190, 210, 225 and 273s. The red dashed line corresponds to L_1 while the blue dashed one to L_2. Image (g) is taken at the end of the drying, at 300s. The orange rectangle corresponds to the zone imaged on the other pictures. (h) Interparticle distance within L_1 (circles) and distance between L_1 and L_2 (triangles).

It has been shown that L_1 is roughly equal to D/tan(θ) (Fig.2c-1), where D and θ are the particle diameter and the contact angle respectively [6]. This expression is related to the capillary force between the particle and the air-water interface. This force prevents particles to go closer towards the CL, beyond L_1, since at shorter distance the air-water interface should be deformed by the particle [6,8,13]. Hereafter, chain-like aggregates grow parallel to the CL as new particles arrive (Fig.1a-b) [6,13] . Since the arrival rate at L_1 is slow (0.5 particle/s) we observe undulation and breakage of the chains between two successive depositions. The growth of the chains relies on two mechanisms. Either adjacent chains grow individually until they get connected to the neighbouring ones or they move along the CL until they come across other chains and merge (see Video V1 in the Supplementary material). The depletion distance L_1 increases with time up to t=200s (full cirles in Fig. 2a and red dashed line in Fig. 1a-c). Therefore particles first come from the droplet centre towards the CL, stop at the line L_1 and then move slowly in the opposite direction, towards the droplet centre, i.e., they undergo a reverse motion [8,13]. L_1 follows an inverse power law of the rescaled time (t_f-t), $L_1=L_0(t_f-t)^{-1}$, where L_0 is the prefactor defined by the contact angle and the particle diameter at the beginning of the drying, $L_0=D/\theta_0$ (Fig.2c-1), and t_f the time when the droplet is completely dried (Fig.2a-inset). As shown by Weon and Je [8], the scaling of L_1 is also directly related to the linear decrease of the contact angle with the rescaled time, $\theta=\theta_0(t_f-t)$. Therefore, the reverse motion of the particles corresponds to a decrease of the contact angle near the CL and the subsequent downward motion of the meniscus, i.e., the thinning of the liquid film in between L_1 and the CL (Fig.2c-2). Before the reverse motion stops, around 160s, some particles get out of the chains and move rapidly and over a short distance in the opposite direction, towards the CL. Those individuals form progressively a second row at a distance L_2 of the CL (blue dotted line in Fig.1c), which is close to the first one (Fig.1d). It is worth noting that in the following, from t=160s, all the particles coming from the droplet centre first flow towards the CL then stop at the line L_1, undergo the reverse motion for a while and then move again in the opposite direction, towards the CL, and stop at a distance L_2 of the CL (insert Fig.2b). We distinguish four consecutives steps:

(I) For 160<t<200s, both L_1 and L_2 increase, the distance between the two rows being constant, around 1.3D; value which is greater than the interparticle distance within L_1 (see in Fig.1h). Therefore we consider that the two rows are independent. We plot on Figure 2b the temporal evolution of the total number of particles at a given time, called the *cumulative number*, that stop at each position L_1 (full circles) and L_2 (open circles). In the first half of the

experiment, up to 160s, particles are deposited only at L_1 with a constant arrival rate (~0.5 particles/s). Above 160s particles start to move from L_1 towards L_2. This is what we call hereafter the *migration process* (Fig.2b-inset and Fig.2c-3). During the next forty seconds (160s<t<200s), the particle arrival rates on both rows are equal (same slope of the curves in Fig.2b). In other words, the number of particles that arrive from the droplet centre up L_1 is equal to the number of particles that leave L_1 in order to go towards L_2, still at around 0.5 particles/s.

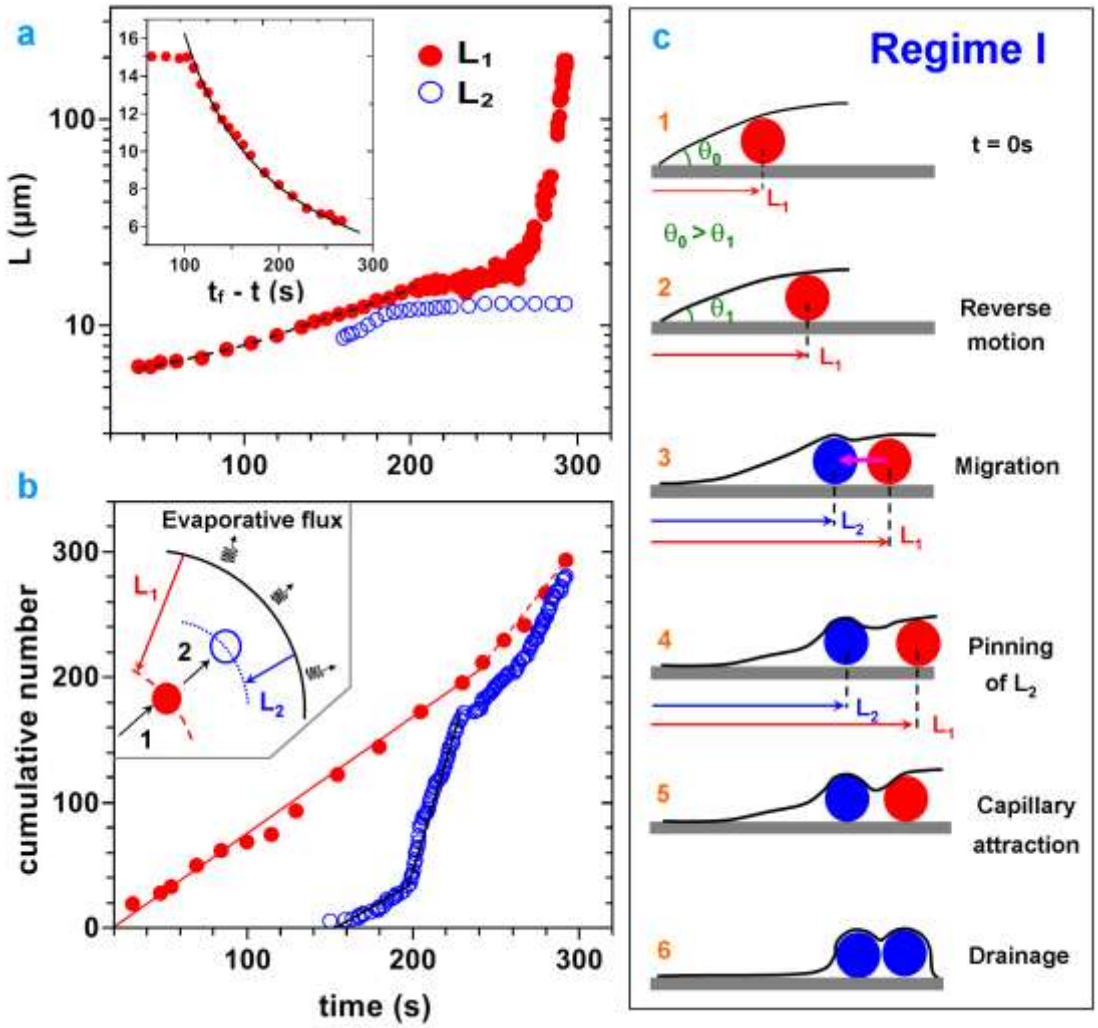

Figure 2: (a) Temporal variation of the position of the rows L_1 (red) and L_2 (blue). The dashed line corresponds to the part of the data fitted in the inset. Inset: Variation of lines L_1 with (t_f-t). The line is an inverse power law of the data. (b) Evolution of the cumulative numbers of particle over time that arrive at L_1 and L_2. The continuous line is a linear fit while the dashed one is a guide for the eyes. Inset: Schematic of the two step arrival of the particles near the CL: particles come from the centre, first deposit at a distance L_1 and then move up to L_2, which corresponds to the migration process. (c) Sketch of the successive steps of the droplet drying. The top scheme corresponds to the first particles deposited at L_1 with a contact angle θ_0. The red and the blue particles belong to L_1 and L_2, respectively.

(II) For 200<t<240s, L_1 keeps increasing while L_2 stops moving. Thus the distance between L_1 and L_2 increases over time until the end (Fig.1h and Fig.2a). The particles flux between the two rows is not equilibrated anymore and the arrival rate from L_1 towards L_2 is eight times greater than the arrival rate from the droplet centre towards L_1. Therefore, we have a rapid depopulation of L_1 until almost all the particles belong to L_2, at t=240s (see videoV2 in the Supplementary material and Fig.1d-e). At that moment, while freshly deposited particles at L_1 still undergo Brownian motion, the vast majority of the particles in L_2 get completely arrested forming distorted chains, those particles being pinned by the meniscus (Fig.2c-4). As the contact angle decreases, we suppose that the liquid film near the CL thins and the air-water interface comes closer to the particles, get strongly deformed and then becomes concave. Rapidly after there is a partial dewetting of the particles located at L_2. This pinning results from a capillary attraction due to the curvature of the film in between particles [14,15] (see Video V2 in the Supplementary material).

(III) Later on, for t>240s and up to the complete drying of the droplet, almost all the new particles that arrive at L_1 , stop there for few seconds (4 up to 10s) and move after towards L_2. However, the position of L_1 with respect to the CL rapidly increases with time while L_2 remains constant, (Fig.2a). Surprisingly, in this case the temporal evolution of the particle arrival rate on both rows is almost the same (Fig.2b), Therefore, since the distance between the two rows increases rapidly (Fig.2a), particles located at L_1 move faster over time towards L_2. As can be seen on Figure 2b, nearly all the particles that arrive at L_1 over the course of the drying also end up at L_2, since the total number of particles at the end is almost the same on both rows.

(IV) Near the end of the drying, for t around 295s, few particles deposit at L_1 (Fig.1a in the Supplementary material). The meniscus in the vicinity of the ring comes closer to the subtstrate (Fig.1b in the Supplementary material) and then breaks-up when touches it (Fig.1c in the Supplementary material), creating in this way two depinning fronts. The first front moves towards the ring (dashed dotted line in Fig.1c in the Supplementary material) and the second one towards the centre (dashed line). This latter front moves discontinuously as it encounters particles in its path and with an average velocity of 1.4±0.6µm/s. This process lasts 30s after which all the liquid is evaporated.

3.2 Regime II

The evolution of the shape of the ring on the overall drying process in the second regime, for ϕ=3.10^{-4} and 10^{-3}, is shown respectively on Fig.3 and Fig.2 in the supplementary material. Two main features of the regime I or also observed in the regime II:

(I) Particles pile up at a distance L_1 of the CL (Fig.3a and Fig.2a in the supplementary material) and L_1 increases over time up to 180s-200s, still with $L_1=L_0(t_f-t)^{-1}$ (Fig.4a). In the present case, L_1 corresponds to the distance between the CL and the outermost row of the ring (red lines in Fig.3a-d). Since the arrival rate at L_1 is around eight times greater than before, a monolayer with several rows is rapidly formed near the CL with an hexagonal structure (Fig.3b).

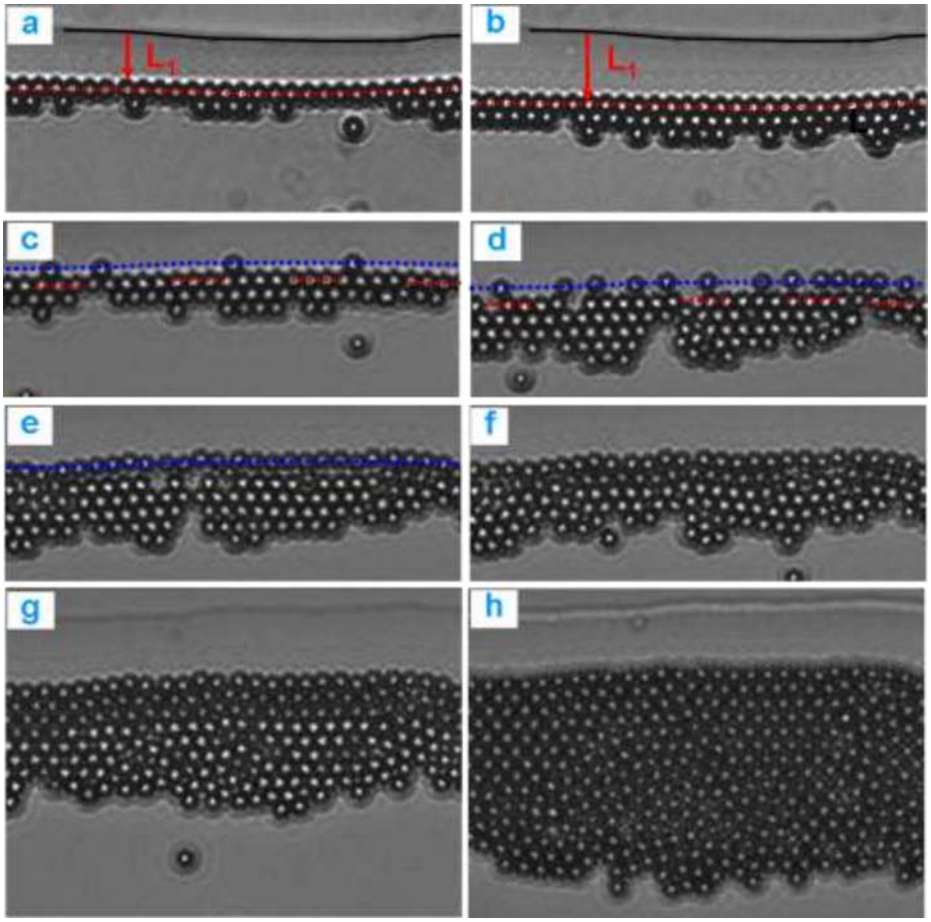

Figure 3: Successive images of the colloidal deposition near the CL for ϕ=3.10^{-4}. The letter for each image corresponds respectively to t=100, 203, 216, 221, 237, 247, 280 and 302s. The red dashed line corresponds to L_1 while the blue dashed one to L_2.

This regular particle arrangement is expected in very high confinement for h<1.1-1.3D, with h the vertical distance between the glass surface and the flat air-water interface [12]. It is worth noting that the hexagonal order is preserved when L_1 increases over time. No defect shows up during this inward motion of the ring (Fig.3b and Fig.2b in the Supplementary material). Actually, we can observe defects within the structure over short periods of time, due to the motion of the crystalline ring towards the droplet centre. However, this motion is rather slow (0.01-0.02μm/s) and the Brownian motion of the particles helps to recover locally an hexagonal order.

(II) Around 140-150s, particles from L_1 start to move towards the CL and form progressively a row even closer to the CL, at a distance L_2 (Fig.3c-d and Fig.1b-c in the Supplementary material). The migration process from L_1 towards L_2 is the same irrespective of ϕ. Indeed, the curves of the temporal evolution of the total (cumulative) number of particles that arrive at L_2 for various ϕ are almost superimposed (Fig. 9b). This number first increases slowly, up to 200s (arrival rate at L_2 of 0.5 particle/s) and more rapidly thereafter (around 4 particles/s) (Fig.4b). This particle motion towards L_2 ends up when the row is full, i.e., there is almost no room to put another particle within this row for t=250s (Fig.3e). We emphasize that the crystalline ring and the row located at L_2 are independent. Indeed, the interparticle distance within L_2 decreases over time as new particles come from L_1 and levels off around D when the row is full, while the interparticle distance in L_1 remains always constant and equal to D (Fig.4b-inset). In addition, the average distance between particles which belong to L_1 and L_2 is not constant. It increases slowly for 140s<t<190s, this distance being always slightly bigger than the interparticle one within L_1, around D. During this period, L_1 and L_2 both increase thus the main ring and the isolated row move towards the droplet centre (reverse motion), the main ring faster than the isolated row. For 190s<t<240s, the distance between L_1 and L_2 decreases down to a value roughly equal to D, i.e., the two rings get in contact. Since the position of L_2 does not change anymore, the main ring thus moves in the opposite direction, towards the CL, until it touches the isolated row and merges to form a unique ring for t=240-245s.

The migration process towards L_2 is a three-step process. Firstly for 140s<t<190s, the migration leads only to local rearrangements in the vicinity of the holes left by the leaving individuals. Particles at L_1 near that places rearrange themselves in such a way that the hexagonal structure is recovered locally (Fig.5a-c). In addition to those movements of single particles there are also rotations of small clusters (three to seven particles) within which the hexagonal order is preserved (Fig.3 in the Supplementary material). Thereafter, larger parts of

the ring are involved in these structural modifications (Fig.5d-e) and the full ring ends up by recovering a hexagonal order. In a second step, for 190s<t<235s, the migration rate becomes higher (Fig.3c-e) while the distance between the main ring and the isolated row decreases slowly (Fig.4b and inset). It is worth noting that the ring structure remains ordered (Fig.3e) and particles still migrate one by one towards L_2. Finally, for 235s<t<245s, there is a cascade of rearrangements within the main ring that drives all its particles towards L_2 (Fig.3f and Video V3 in the Supplementary material).

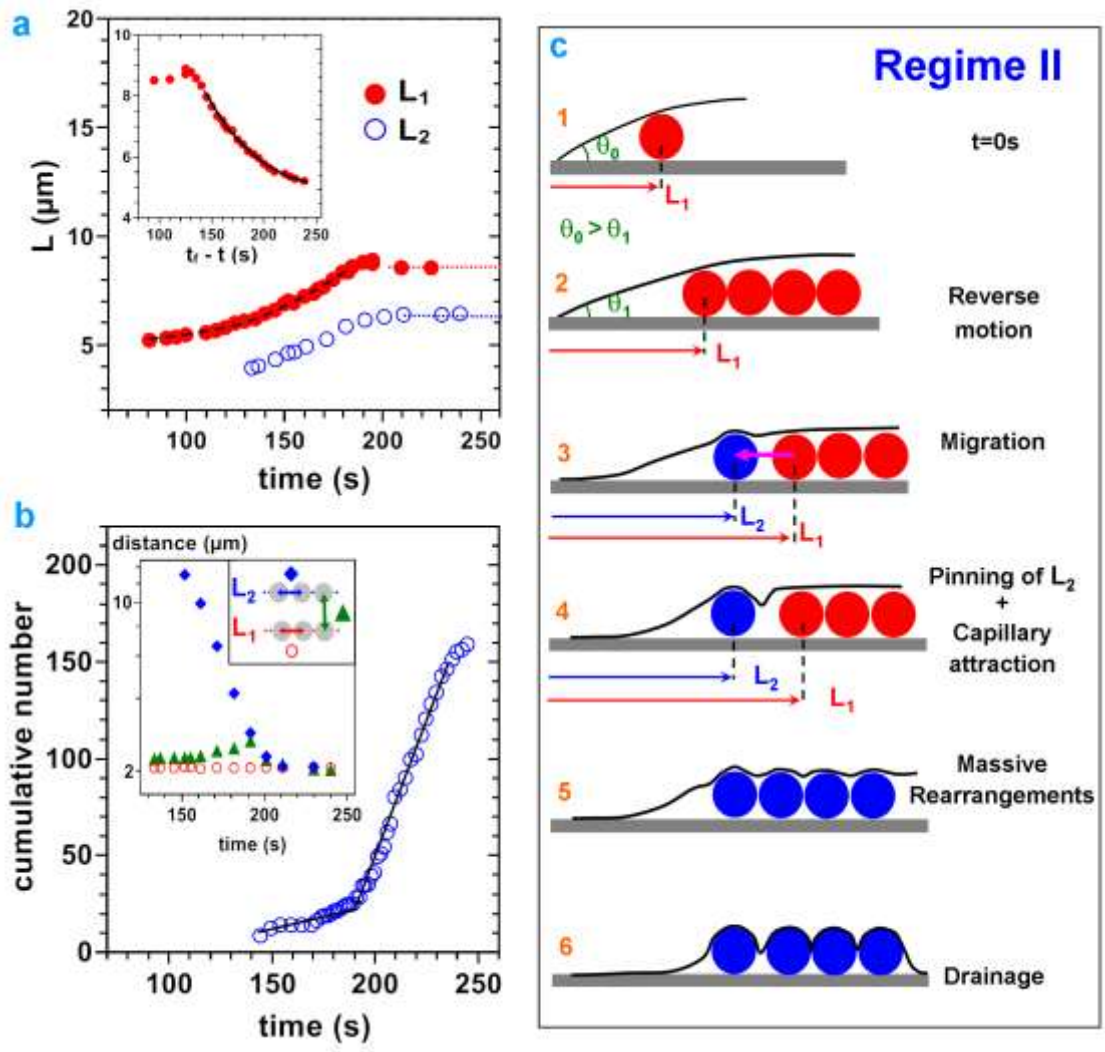

Figure 4: (a) Temporal variation of the position of L_1 and L_2 for ϕ=3.10^{-4}. The dashed line corresponds to the range of data fitted in the inset. Inset: The same data for L_1 plotted against (t_f-t). The continuous line is an inverse power law fit of the data. (b) Variation of the number of particles over time that move from L_1 towards L_2. The two lines are guides for the eyes. Inset: Variation of the interparticle distance within the main ring (circles), within the isolated row (lozenges) and between L_1 and L_2 (triangles). (c) Sketch of the successive steps of the droplet drying. The top scheme corresponds to the first particles deposited at L_1 with a contact angle θ_0.

These massive rearrangements lead to the formation of a single ring with a rather disordered structure. Rapidly thereafter, motions of larger clusters of particles within this ring also help to recover locally a hexagonal order (video V3 in the Supplementary material). A similar behaviour is observed during the latest stages of the particle migration for higher volume fractions (see Video V4 in the Supplementary material for ϕ=10^{-3}). In this case, since the width of the main ring is even greater than before, more particles are involved in the massive rearrangement events.

In the following, for t>250s and up to the end of the drying process, particles coming from the droplet centre simply accumulate at the innermost part of the ring, forming in this way an hexagonal monolayer ring. As previously this ordered structure indicate to us that the monolayer remains confined, the height of the liquid film h being slightly larger than D [16]. We thus conclude that the meniscus progressively spreads on the ring as it grows. Indeed, the meniscus moves towards the droplet centre and the water film between the particles becomes progressively smaller than the particle diameter and thus particles get pinned and the capillary attraction forces between particles takes place within the ring (Fig.5 in the Supplementary material). Once particles come in contact with the ring front they almost do not move. Indeed, we observe very few rearrangements near the growing front of the ring until the end of the process (Fig.4 in the Supplementary material).

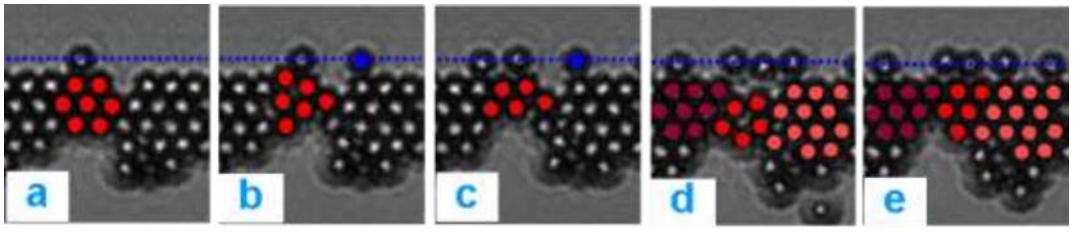

Figure 5: Rearrangement of the particles within the first ring (red particles) due to the motion of some individuals towards the second ring (blue particles) for image a to c. The ring recovers a hexagonal symmetry over longer distances on images d and e.

During this piling up process in the inner part of the ring, the particles in the outermost part get progressively immobilized (Fig.5a-b in the Supplementary material). This event is due to the motion of the meniscus close to the CL: it moves downward as it spreads over the ring, starting from its outermost part, and comes into contact with the particles. The thickness of the water film becomes smaller than the particle diameter, and thus the particles are not completely immersed as before and they get pinned in this way [17]. Later on, the trapping becomes spatially heterogeneous (Fig.4c-f in the Supplementary material), some particles

being partially trapped (darker ones) while those in their vicinity are not in contact with the meniscus (white ones). Finally, at the very end of the drying, a part of the meniscus touches the solid surface in between innermost part of the ring and the centre (Fig.5f in the Supplementary material). The break up of the meniscus creates two dewetting fronts, the first one moving towards the CL while the other moves in the opposite direction, towards the centre. Once the former front has encountered the ring we do not observe any noticeable change of its internal structure (Fig.5h in the Supplementary material).

For higher ϕ ($\phi > 10^{-3}$) the spreading of the meniscus on top of the ring brings about significant modification of the colloidal structure (Fig.6). At the beginning of the drying, a monolayer is still formed. For t>30s particles start to pile up on one another forming locally two layers, in the innermost part of the ring (Fig.2a in the Supplementary material). The packing is hexagonal within the monolayer while it is square inside the two layers. This change of symmetry from hexagonal to square, also observed by Marin et al. [7], is due to a decrease of the particle confinement [16,18] when one goes from the CL towards the droplet centre. Suprisingly, as new particles accumulate on the innermost part of the ring, the width of the two-layers zone remains almost constant while the width of the monolayer zone increases. Indeed, the limit between the two zones (dashed lines in Fig.2a-d in the Supplementary material) moves towards the droplet centre. Later on, the width of the two-layers zone decreases over time until we get only a monolayer ring at the end of the experiment (Fig.2e-f in the Supplementary material).

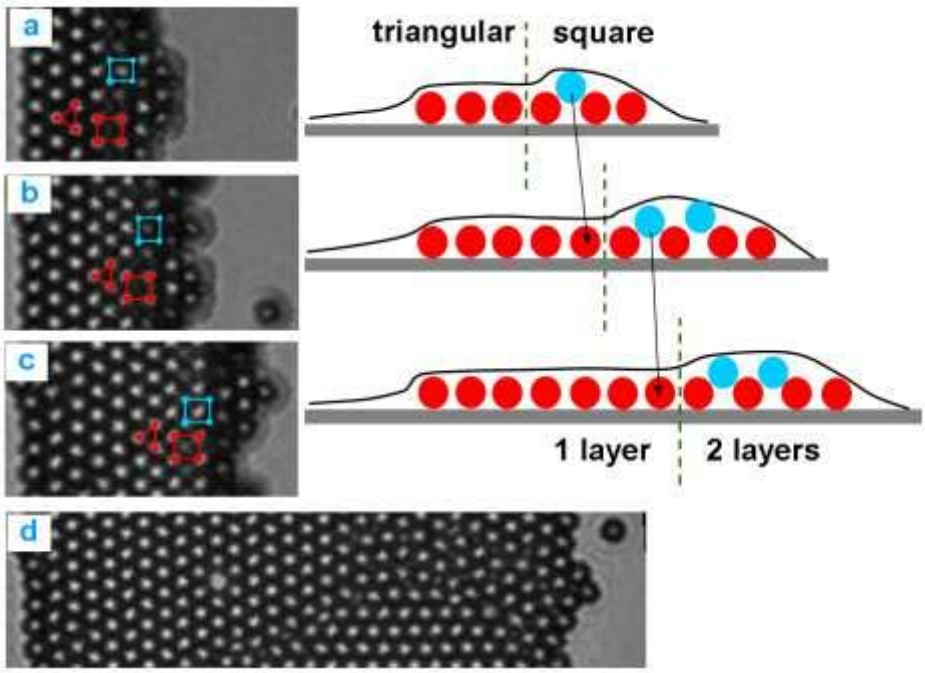

Figure 6: Structural changes due to the spreading of the meniscus over the ring for $\phi=10^{-3}$. (a) In the first three rows of the ring, from the CL, there is a monolayer with an hexagonal ordering (red triangle) while the other rows particles adopt a square ordering on both layers. The blue and the red squares correspond to particles belonging to the top and the bottom layer, respectively. From image a to b and from b to c, some particles previously on the top layer move downwards and eventually belong to the bottom layer (blue particles on the schematics on the left). We also see clearly that at the end of the drying process (image d) all the particles are disposed within a monolayer, with the hexagonal symmetry.

Therefore one can conclude that on the course of the experiment there is a progressive flattening of the ring which starts from its outer part. Since this process is rather slow we can easily follow the associated structural changes, i.e., the square to hexagonal transition, as shown in Fig. 6. Particles that belong to the top layer and which are close to the monolayer zone, move towards the glass slide (blue particles in Fig.6a). During this downward motion the distance between particles on both layers increases, i.e., the mesh size of the square lattices increases. Hereafter, particles of the top layer eventually come into contact with the glass slide and thus we get only a monolayer. During this last motion the square packing evolves progressively towards the hexagonal one (Fig.6a-b and b-c). The flattening of the ring ends up well before the end of the experiment (t=250s) and the subsequent accumulation process of particles simply leads to the widening of the hexagonal monolayer ring. Here again, at the end of the drying the meniscus comes into contact with the glass slide, breaks up just a head of the innermost part of the ring, and one part of the two dewetting fronts move in opposite direction (Fig.1 in the Supplementary material). The structure of the ring is not modified during this very last stage of the drying (Fig.5f-h in the Supplementary material).

Finally, for the highest ϕ we used (ϕ=5.10^{-3}), the evolution of the structural properties of the ring is quite similar, expect that we obtain a multiple-layers ring at the end of the drying (Fig.6 in the Supplementary material). The motion of the liquid meniscus from the CL towards the droplet centre over the time flattens out the ring, except may be in its central part. From t=100s, there is first the spreading of the ring, at its outer part, corresponding to the square (two layers) to hexagonal (monolayer) just described above, that leads to the widening of the monolayer in the vicinity of the CL (Fig.6a-b in the Supplementary material). Hereafter, when we depart from the CL, hexagonal to square transitions also occur (rectangles in Fig.6b-c in the Supplementary material). In this case, the number of layers remains the same, either three or four layers, but the local height of the ring decreases due to the change of crytalline structure of the layers [18]. Much later, near the end of the drying and just before one part of the meniscus touches down the glass slide, there is a important flattening of the ring, at its inner part. While at this place the ring was two to three layers high it rapidly flattens out and spreads towards the centre until we get a monolayer (Fig.6c-e in the Supplementary material).

We also changed the evaporation rate to check the generality of our results so far on the dynamics of the particles near the CL. We confined the sessile droplet by putting a glass plate on top of it (Fig.7a in the Supplementary material). By varying the height of this plate relative to the top of the droplet we can finely control the evaporation rate and we explored in this way lower evaporation regimes (greater t_f). The evaporation rate decreases with the air gap in between the top of the droplet and the plate (Fig.7b in the Supplementary material). We focus here on ϕ=10^{-3}, but similar results were obtained for other ϕ. The same successive steps of the ring formation are observed when the evaporation rate is changed: (i) the reverse motion of L_1, (ii) the formation of L_2, (iii) the flattening of the ring over time (Fig.8 in the Supplementary material). The related dynamics of each of those phenomena slows down when the evaporation rate decreases. L_1 follows the inverse power law variation over the rescaled time, $L_1=L_0(t_f-t)^{-1}$, as before (Fig.7a-inset). This means that the reverse motion of L_1 still corresponds to the linear decrease of the contact angle with the rescaled time. The more the droplet is confined the slower the contact angle decreases. It is worth noting that the maximum amplitude of the reverse motion of the main ring is the same, irrespective of the evaporation rate in confined case, while it is twice the value we found previously in the non confined case (Fig.7a). In addition, the curves for the temporal variation of L_1 for the various confinements fall on a master curve when plotted against t/t_f. The reverse motion stops around t/t_f=0.6 for both the confined and non confined cases (Fig.7b). The migration process from L_1

towards L_2 also occurs later on when the evaporation rate decreases (Fig.7b) and we also get a master curve for the number of particles that migrate towards L_2 for different confinements (Fig.7c). Here again, the lower the drying rate the slower the migration rate.

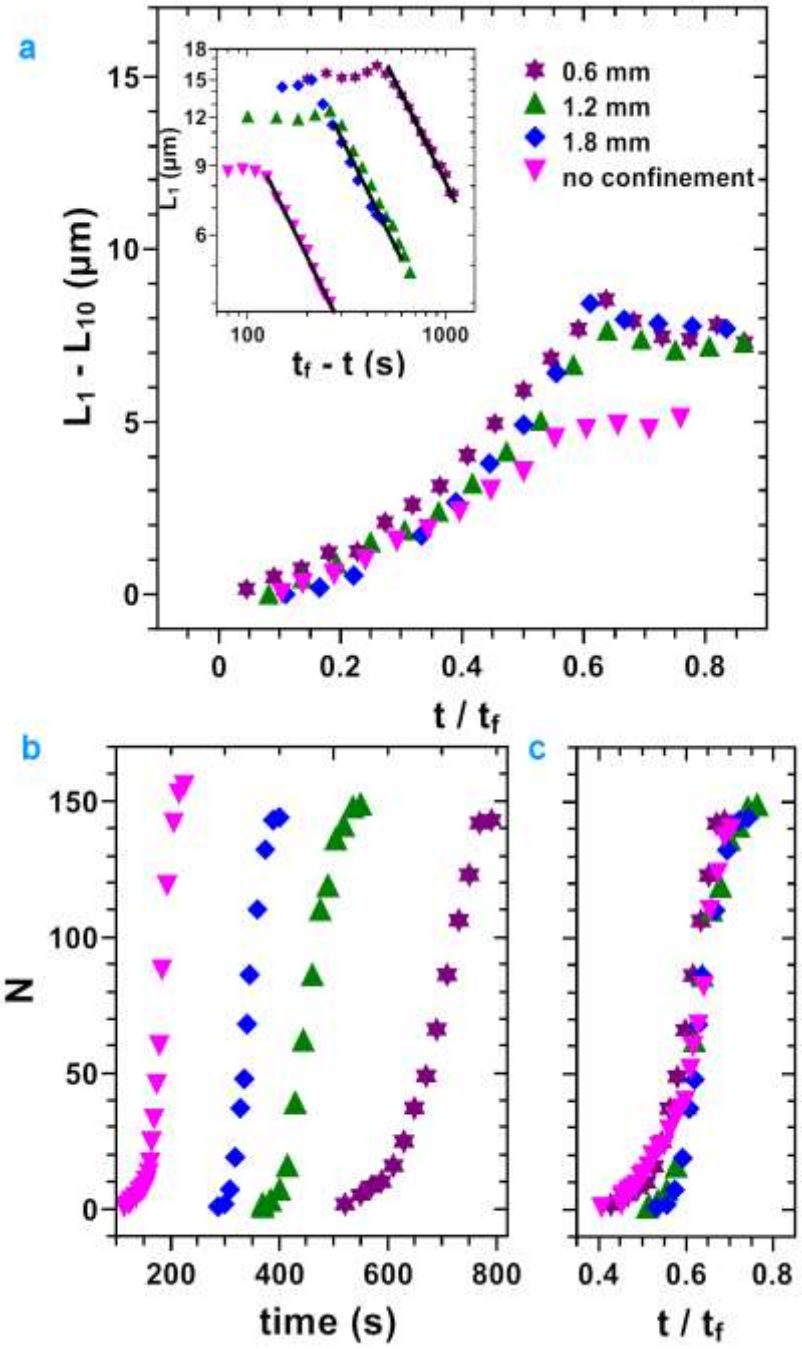

Figure 7: (a) Variation of to the position L_1 with (t/t_f) for lower evaporation rates. L_{10} is the initial position of L_1. Inset: The same data plotted against $(t_f\text{-}t)$. The continuous lines are inverse power law fits of the data. (b) Temporal evolution of the number of particles over time that migrate from L_1 first ring towards L_2 for the various evaporation rates. (c) The same data than in b but rescaled by plotted against (t/t_f).

4. Discussion

We have seen that the first step of the coffee stain formation, for a wide range of ϕ and also different evaporation rates corresponds to the deposition of particles near the CL and their subsequent slow reverse motion, towards the droplet centre. Thus, we may conclude, even though we do not measure the variation of the apparent contact angle, that the reverse motion of the particles is due to the thinning of the meniscus near the CL, whatever the piling-up kinetics of the particles near the CL and the structure of the ring as L_1 increases [6,8,13,19]. During this reverse motion, the evaporative flux that draws particles near the droplet edge, is not great enough to allow the deformation of the meniscus around the particles located at L_1, which could lead to the particle trapping at that place [6]. Instead as the liquid meniscus thins over time near the CL it repels the particles of the ring towards the droplet centre keeping its convex shape (Fig.2c1-2 and Fig.4c1-2), as observed by Weon and Je [8] . This remains valid whatever the width of the ring since the capillary force that repels the particles acts only on the outermost row of the ring. Indeed, the reverse motion takes place over the same range of time and up to t=180-200s, for various ϕ (Fig.8a). The formation of L_2 closer to the CL and its temporal evolution are also quite similar for

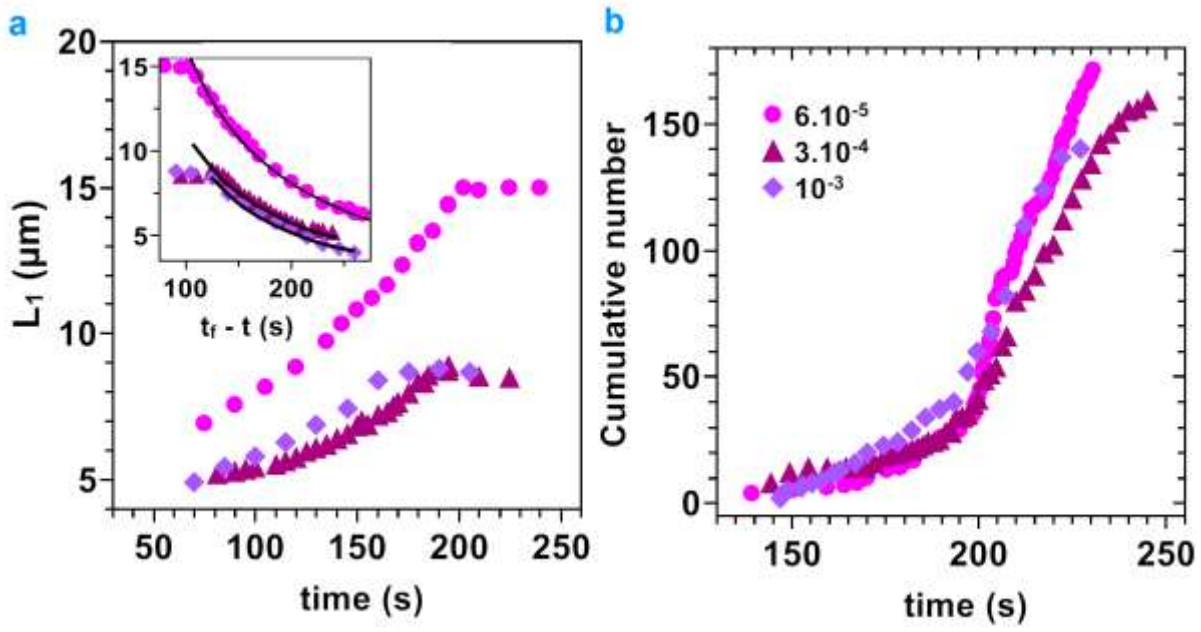

Figure 8: (a) Temporal variation of to deposition lines L_1 for ϕ=6.10^{-5}, 3.10^{-4} and 10^{-3}. Inset Same data plotted against (t_f-t). Lines are inverse power law of the data. (b) Variation of the total number of particles over time that move from the first ring to the second for various ϕ. The data for ϕ=6.10^{-5} and *3.10^{-4}* are also shown on Fig. 2b and Fig.4b.

various ϕ. Besides, L_2 shows up before L_1 starts to level off, for t=160s, and like L_1, L_2 moves towards the droplet centre until t=200s (Fig.2a and Fig.4a). During that time interval (160s<t<200s), the distance between L_1 and L_2 is almost constant in the regime I (Fig.1h) while it slightly increases in the regime II (Fig.2b-inset), but in anycase this distance remains small and never exceeds 1.3D. For larger times, for t>200s, the position of L_2 does not change anymore until the end of the drying. Likewise, the particles at L_2 get still. We suppose that the meniscus in the vicinity of the particles is deformed; its shape becomes concave and particles start to protude through the air-water interface (Fig.2c-3 and Fig.4c-3). At that moment the evaporation rate near the CL is thus strong enough to allow the deformation of the meniscus and the subsequent pinning of the particles. This pinning event at L_2 is responsible of massive and continuous migrations from L_1 towards L_2. There is an eigthfold increase of the migration rate from t=200s for all the ϕ (Fig.8b). In both regimes this massive migration ends up by the accumulation of particles in a single ring, with its outermost row located at L_2 (Fig.2c-5 and Fig.4c-5). The building up dynamics of this final ring depends strongly on ϕ. For $\phi < 10^{-4}$ (regime I), the migration towards L_2, to form a single thicker ring, is entirely due to the capillary attraction. Particles first stop at L_1, follow the reverse motion of this row, like the other particles that were already present at L_1. Then, they move towards L_2, being attracted one by one by the capillary force due to curvature of the meniscus in between L_1 and L_2 [20]. Actually, the height of this meniscus is smaller than the particle diameter D, i.e, the meniscus has a concave shape in between the particles (Fig.2c-5). The way the ring is formed here at L_2 is also due to the fact that we can not build a ring at L_1, due to the small arrival rate of particles at this place on the overall experiment. Indeed, the average time between successive arrivals at L_1 is smaller than the time for a particle to goes from L_1 towards L_2 by capillary attraction, since the slope of curve of the cumulative number for L_1 is always smaller than that of L_2 (Fig.2b). Moreover, the capillary attraction between particles of the two rows starts well before the end on the drying (around t=200s) and about 90% of the particles coming from the droplet centre stop at L_1 and end up at L_2 by this attraction mechanism. For the regime II ($5.10^{-3} > \phi > 10^{-4}$), the ring formation results from two consecutive steps:

1- The structure of the main ring remains hexagonal during the migration towards L_2 since rearrangements are quick enough to recover locally an ordered structure. But at the end of this process (t=235s for instance for ϕ=3.10^{-4}) the particles at L_2 get pinned and there is again a capillary attraction between the particles belonging to each row. This induces a serie of

massive rearrangements, that involves all the particles belonging to the main ring and leads to the rows merging in less than 10s (see Video 3 in the Supplementary material).

2- Later on, most of the particles inside the droplet (65 to 80% depending on ϕ) are not yet deposited, i.e, they are not arrived near the CL. Those ones simply accumulate at the inner part of the ring in an ordered manner, up to the end of the drying, since particles are able to rearrange themselves rapidly at the growth front of the ring. However there are few defaults in the ring structure but those ones are chiefly due to the presence of few out of range particles. While new particles accumulate at the inner part of the ring, the meniscus pinned at L_2 is deformed and spreads over the ring, the dynamics of those two phenomena being completely non coupled: particles accumulate faster on the ring than the meniscus moves along the ring towards the droplet centre. For $\phi=3.10^{-4}$, the movement of the meniscus does not modify the structure of the ring resulting from the particle accumulation. For $\phi=10^{-3}$, a two-layers ring rapidly grows near the CL early in the drying process (Fig.2a in the Supplementary material), since the rate of particle accumulation at the ring is greater than before and the decrease of the contact angle over time remains the same. The deformation of the meniscus over time flattens out the ring until we get a monolayer (Fig.6). For even greater particle volume fraction, for $\phi=5.10^{-3}$, the multi-layers ring is first flatten at its outer edge and progressively over its full width, ending by its inner part when the meniscus touches the substrate. We end up with ring that has a asymmetric cross-sectional shape, similar to those obtained during the band formation in the dip-coating experiments [21]. The evolution of the droplet shape near the CL for the regime II is in qualitative agreement with the experiments performed by Parisse and Allain [22,23] and the theory developped by Kaplan and Mahadevan [11], even though both studies considered higher initial volume fractions and thus deposits with much greater sizes.

Interestingly, we do not observed any order to disorder transition in the ring structure during the drying process as observed by Marin et al. on post mortem dried droplet [7]. Instead, we have a disorder to order transition with respect to ϕ. For $\phi<10^{-4}$, the ring has a disordered structure due to the capillary attraction while for $\phi>10^{-4}$ the structure is well ordered, the final structure of ring depending also on meniscus deformation near the droplet edge. Moreover, we cannot establish any relationship between the particle velocity near the CL and the internal ring structure as put forward by Marin et al. to explain an evolution of the ring structure as the droplet dries. We determined the average particle velocity, U, over the entire experiment for all the particles about to be deposited for all ϕ (Fig. 9b). The overall temporal evolution of U is qualitatively similar to what was observed by Marin et al. In the first part of the drying, for

t<220s, U is almost constant while later on U increases significantly. However the place where U is measured, relative to the inner front of the ring is not the same in both studies. In the case of Marin et al., U is measured at a fixed distance of the CL (174µm). In this configuration the distance between the innermost part of the ring and the position where U is measured decreases over time, as the ring grows. This can partly explained why they observed an increase of U over time, since the closer of the CL the faster the particles move. In our case, we followed the method used by Monteux and Lequeux [6] and we determined the value of U at a fixed distance (30µm) of the innermost part of the growing ring (Fig.9a). Therefore as the ring grows towards the droplet centre the position of the velocity measurement departs from the CL. In the regime I this increase of distance is due to the downward motion of the meniscus that pushes the row L_1 towards the droplet centre, while in the regime II the increase is related to the growth of the ring by accumulation of particles. Since we get the same temporal evolution of U for all ϕ we can conclude that the kinetics of particle deposition depends neither on ϕ nor on the volume fraction of the particles inside the deposit.

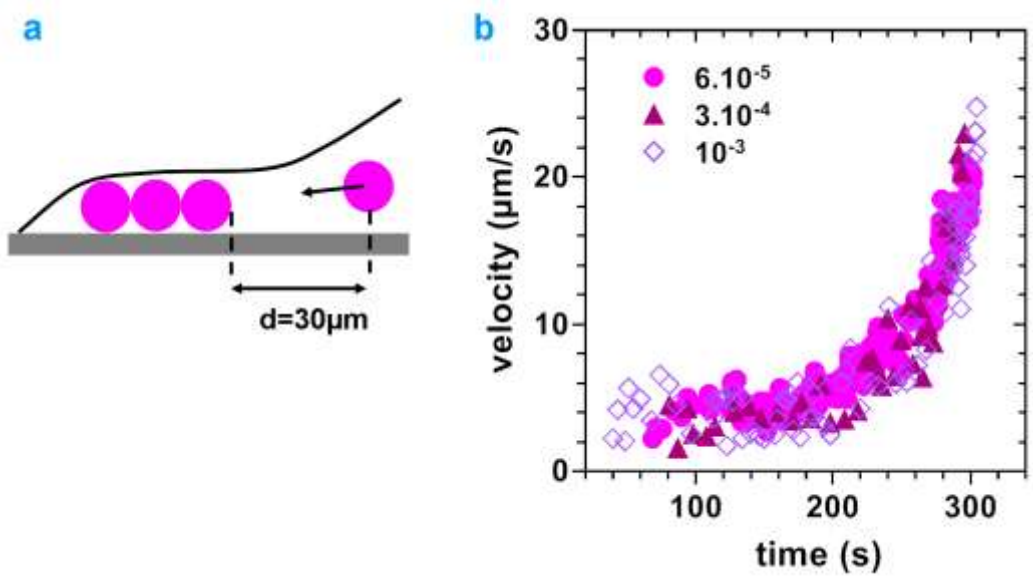

Figure 9: (a) sketch of the position d from the innermost part of the ring, where we measured the average particle velocity. The distance d is constant and equals to 30µm. (b) Temporal evolution of the average particle velocity versus the drying time for $\phi = 6.10^{-5}$, 3.10^{-4} *and* 10^{-3}.

In the first part of the drying, for t<250s, the ring formation is ruled by the deformation of the liquid meniscus, that keeps a convex shape. Later on, the particles velocity increases significantly when the outermost part of the ring becomes pinned by the meniscus. This

indicates to us that in our case the so called *rush hour effect*, corresponding to the velocity increase, is related to the evolution of the shape of the meniscus and its motion towards the glass slide. Actually, the progressive dewetting of the deposit is another source of evaporation which comes in addition to the regular one near the CL. Besides, we could have observed the order to disorder transition mentionned previously in ref.6 if we have worked with a higher number of particles within the droplet, either by increasing ϕ, keeping the same droplet volume as before (0.6µl) or by increasing both ϕ and the droplet volume. Indeed, Marin et al. worked with a droplet volume of 3µl and $\phi > 10^{-2}$, using the same particle size. Finally, we always get a single ring at the end of the drying whatever ϕ (Fig. 9 in the Supplementary material). It turns out that the volume of the droplet we used do not allow the formation of multiple rings. Indeed, for almost the same conditions than ours (droplet of water deposited on glass slide and micrometer polystyrene particles) and for a 1µl droplet, Shmuylovich et al. [12] also got a single ring while they obtained multiple rings for larger droplet volumes, higher than 8µl. Note that multiple rings are more often observed for smaller particles and for a wider range of droplet volumes and ϕ [9,10]. This is probably due to the fact that the deformation of meniscus in the vicinity of the particles that leads to the particle pinning is easier when the particles are smaller. In addition, smaller particles can also move closer to the moving CL, i.e., the depletion length is smaller, and thus the downward motion of the meniscus prior touching the substrate is reduced and thus takes place more rapidly [24].

5. Conclusions

We report on the drying of colloidal suspension droplet deposited on a glass slide. We used dilute solutions which allow us to follow the formation of the ring at the particle scale in the vicinity of the CL since the very beginning of the drying process. We find that particles first accumulate near the CL and reverse their motion towards the droplet centre. This reverse motion is directly related to the decrease of the contact angle. Later on, depending on the particle volume fraction, we found that there are two ways of forming a coffee stain. For $\phi < 10^{-4}$, the particle can pile up in order to form a ring full of particles. Unfortunately the kinetics of this colloidal assembly is not fast enough to form a permanent ring. As the meniscus is deformed and moves towards the substrate, particles draw near the CL, get pinned and form in this way a new ring with a disordered structure. For $\phi > 10^{-4}$, the colloidal ring grows more rapidly and thus earlier in the drying process. The deformation of the meniscus,

prior to the depinning of the CL, leads to structural changes within the ring. The value of ϕ at the transition corresponds to the parameters we fixed. Therefore, if for instance we lower the RH [25], decrease the particle size [26] or modify the DLVO [27] and depletion interactions [28] we will change the dynamics of both the particle piling-up and the meniscus deformation, which in turn will modify the ϕ value at the transition. The present work can also be useful to understand the structure and the shape of deposits obtained during the dip-coating process for instance.

References

[1] U. Thiele, Patterned deposition at moving contact lines, Adv. Colloid Interface Sci. 206 (2014) 399–413. doi:10.1016/j.cis.2013.11.002.

[2] R.D. Deegan, O. Bakajin, T.F. Dupont, G. Huber, S.R. Nagel, T.A. Witten, Capillary flow as the cause of ring stains from dried liquid drops, Nature. 389 (1997) 827–829. doi:10.1038/39827.

[3] R.D. Deegan, O. Bakajin, T.F. Dupont, G. Huber, S.R. Nagel, T.A. Witten, Contact line deposits in an evaporating drop, Phys. Rev. E. 62 (2000) 756–765. doi:10.1103/PhysRevE.62.756.

[4] K. Sefiane, Patterns from drying drops, Adv. Colloid Interface Sci. 206 (2014) 372–381. doi:10.1016/j.cis.2013.05.002.

[5] B.M. Weon, J.H. Je, Self-Pinning by Colloids Confined at a Contact Line, Phys. Rev. Lett. 110 (2013) 28303. doi:10.1103/PhysRevLett.110.028303.

[6] C. Monteux, F. Lequeux, Packing and Sorting Colloids at the Contact Line of a Drying Drop, Langmuir. 27 (2011) 2917–2922. doi:10.1021/la104055j.

[7] Á.G. Marín, H. Gelderblom, D. Lohse, J.H. Snoeijer, Order-to-Disorder Transition in Ring-Shaped Colloidal Stains, Phys. Rev. Lett. 107 (2011) 85502. doi:10.1103/PhysRevLett.107.085502.

[8] B.M. Weon, J.H. Je, Capillary force repels coffee-ring effect, Phys. Rev. E. 82 (2010) 15305. doi:10.1103/PhysRevE.82.015305.

[9] E. Adachi, A.S. Dimitrov, K. Nagayama, Stripe Patterns Formed on a Glass Surface during Droplet Evaporation, Langmuir. 11 (1995) 1057–1060. doi:10.1021/la00004a003.

[10] R.D. Deegan, Pattern formation in drying drops, Phys. Rev. E. 61 (2000) 475–485. doi:10.1103/PhysRevE.61.475.

[11] C.N. Kaplan, L. Mahadevan, Evaporation-driven ring and film deposition from colloidal droplets, J. Fluid Mech. 781 (2015). doi:10.1017/jfm.2015.496.

[12] L. Shmuylovich, A.Q. Shen, H.A. Stone, Surface Morphology of Drying Latex Films: Multiple Ring Formation, Langmuir. 18 (2002) 3441–3445. doi:10.1021/la011484v.

[13] A.S. Sangani, C. Lu, K. Su, J.A. Schwarz, Capillary force on particles near a drop edge resting on a substrate and a criterion for contact line pinning, Phys. Rev. E. 80 (2009) 11603. doi:10.1103/PhysRevE.80.011603.

[14] P.A. Kralchevsky, K. Nagayama, Capillary interactions between particles bound to interfaces, liquid films and biomembranes, Adv. Colloid Interface Sci. 85 (2000) 145–192. doi:10.1016/S0001-8686(99)00016-0.

[15] F. Shao, T.W. Ng, J. Efthimiadis, A. Somers, W. Schwalb, Evaporative micro-particle self assembly influenced by capillary evacuation, J. Colloid Interface Sci. 377 (2012) 421–429. doi:10.1016/j.jcis.2012.02.071.
[16] P. Pieranski, L. Strzelecki, B. Pansu, Thin Colloidal Crystals, Phys. Rev. Lett. 50 (1983) 900–903. doi:10.1103/PhysRevLett.50.900.
[17] N.D. Denkov, O.D. Velev, P.A. Kralchevsky, I.B. Ivanov, H. Yoshimura, K. Nagayama, Two-dimensional crystallization, Nature. 361 (1993) 26–26. doi:10.1038/361026a0.
[18] B. Pansu, P. Pieranski, P. Pieranski, Structures of thin layers of hard spheres : high pressure limit, J. Phys. 45 (1984) 331–339. doi:10.1051/jphys:01984004502033100.
[19] V.H. Chhasatia, Y. Sun, Interaction of bi-dispersed particles with contact line in an evaporating colloidal drop, Soft Matter. 7 (2011) 10135. doi:10.1039/c1sm06393f.
[20] P.. Kralchevsky, V.. Paunov, I.. Ivanov, K. Nagayama, Capillary meniscus interaction between colloidal particles attached to a liquid—fluid interface, J. Colloid Interface Sci. 151 (1992) 79–94. doi:10.1016/0021-9797(92)90239-I.
[21] C.N. Kaplan, N. Wu, S. Mandre, J. Aizenberg, L. Mahadevan, Dynamics of evaporative colloidal patterning, Phys. Fluids. 27 (2015) 92105. doi:10.1063/1.4930283.
[22] F. Parisse, C. Allain, Drying of Colloidal Suspension Droplets: Experimental Study and Profile Renormalization, Langmuir. 13 (1997) 3598–3602. doi:10.1021/la951521g.
[23] F. Parisse, C. Allain, Shape Changes of Colloidal Suspension Droplets during Drying, J. Phys. II. 6 (1996) 1111–1119. doi:10.1051/jp2:1996119.
[24] C. Hsueh, C.L. Moraila Martínez, F. Doumenc, M.A. Rodríguez-Valverde, B. Guerrier, Self-assembly in drying complex fluid at low capillary number, Chem. Eng. Process. Process Intensif. 68 (2013) 64–68. doi:10.1016/j.cep.2012.07.006.
[25] X. Xu, L. Ma, D. Huang, J. Luo, D. Guo, Linear growth of colloidal rings at the edge of drying droplets, Colloids Surf. Physicochem. Eng. Asp. 447 (2014) 28–31. doi:10.1016/j.colsurfa.2014.01.068.
[26] A. Askounis, K. Sefiane, V. Koutsos, M.E.R. Shanahan, The effect of evaporation kinetics on nanoparticle structuring within contact line deposits of volatile drops, Colloids Surf. Physicochem. Eng. Asp. 441 (2014) 855–866. doi:10.1016/j.colsurfa.2012.10.017.
[27] R. Bhardwaj, X. Fang, P. Somasundaran, D. Attinger, Self-Assembly of Colloidal Particles from Evaporating Droplets: Role of DLVO Interactions and Proposition of a Phase Diagram, Langmuir. 26 (2010) 7833–7842. doi:10.1021/la9047227.
[28] R.W. Perry, M.C. Holmes-Cerfon, M.P. Brenner, V.N. Manoharan, Two-Dimensional Clusters of Colloidal Spheres: Ground States, Excited States, and Structural Rearrangements, Phys. Rev. Lett. 114 (2015). doi:10.1103/PhysRevLett.114.228301.